The Metastasis-Promoting Phosphatase PRL-3 Shows Activity toward Phosphoinositides

10 AUTHORS, INCLUDING:

Xun Li
Guangzhou Medical University
258 PUBLICATIONS **2,778** CITATIONS

SEE PROFILE

Jancy Nixon Abraham
Indian Institute of Science Education and Re…
9 PUBLICATIONS **126** CITATIONS

SEE PROFILE

Pablo Ríos
European Molecular Biology Laboratory
11 PUBLICATIONS **146** CITATIONS

SEE PROFILE

Maja Köhn
European Molecular Biology Laboratory
**50** PUBLICATIONS **1,506** CITATIONS

SEE PROFILE

The Metastasis-Promoting Phosphatase PRL-3 Shows Activity toward Phosphoinositides

Victoria McParland,[†] Giulia Varsano,[†] Xun Li,[‡] Janet Thornton,[‡] Jancy Baby,[†] Ajay Aravind,[†] Christoph Meyer,[†] Karolina Pavic,[†] Pablo Rios,[†] and Maja Köhn[†,*]

[†]European Molecular Biology Laboratory, Genome Biology Unit, Meyerhofstrasse 1, 69117 Heidelberg, Germany
[‡]European Molecular Biology Laboratory-European Bioinformatics Institute, Wellcome Trust Genome Campus, Hinxton, Cambridge CB10 1SD, United Kingdom

ABSTRACT: Phosphatase of regenerating liver 3 (PRL-3) is suggested as a biomarker and therapeutic target in several cancers. It has a well-established causative role in cancer metastasis. However, little is known about its natural substrates, pathways, and biological functions, and only a few protein substrates have been suggested so far. To improve our understanding of the substrate specificity and molecular determinants of PRL-3 activity, the wild-type (WT) protein, two supposedly catalytically inactive mutants D72A and C104S, and the reported hyperactive mutant A111S were tested in vitro for substrate specificity and activity toward phosphopeptides

and phosphoinositides (PIPs), their structural stability, and their ability to promote cell migration using stable HEK293 cell lines. We discovered that WT PRL-3 does not dephosphorylate the tested phosphopeptides in vitro. However, as shown by two complementary biochemical assays, PRL-3 is active toward the phosphoinositide $PI(4,5)P_2$. Our experimental results substantiated by molecular docking studies suggest that PRL-3 is a phosphatidylinositol 5-phosphatase. The C104S variant was shown to be not only catalytically inactive but also structurally destabilized and unable to promote cell migration, whereas WT PRL-3 promotes cell migration. The D72A mutant is structurally stable and does not dephosphorylate the unnatural substrate 3-O-methylfluorescein phosphate (OMFP). However, we observed residual in vitro activity of D72A against $PI(4,5)P_2$, and in accordance with this, it exhibits the same cellular phenotype as WT PRL-3. Our analysis of the A111S variant shows that the hyperactivity toward the unnatural OMFP substrate is not apparent in dephosphorylation assays with phosphoinositides: the mutant is completely inactive against PIPs. We observed significant structural destabilization of this variant. The cellular phenotype of this mutant equals that of the catalytically inactive C104S mutant. These results provide a possible explanation for the absence of the conserved Ser of the PTP catalytic motif in the PRL family. The correlation of the phosphatase activity toward $PI(4,5)P_2$ with the observed phenotypes for WT PRL-3 and the mutants suggests a link between the $PI(4,5)P_2$ dephosphorylation by PRL-3 and its role in cell migration.
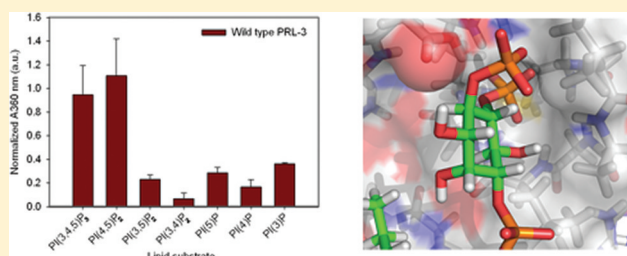
Dual-specificity phosphatases (DSPs) belong to the superfamily of protein tyrosine phosphatases (PTPs). Classical PTPs remove a phosphate from tyrosine residues of proteins, whereas DSPs exhibit activity toward a variety of different substrates such as phosphoserine, -threonine, and -tyrosine but also phosphatidylinositol phosphates (PIPs). The DSP PRL-3 is a cancer biomarker and promising therapeutic target.[1,2] PRL-3 is involved in cell growth, proliferation, and invasion,[1−4] and it is consistently overexpressed in colorectal cancer metastases.[5] It has also been shown to play a causative role in other cancer types and to correlate with increased metastatic potential and poorer prognoses.[1,2] In normal tissue, it is expressed at basal levels in skeletal muscle and the heart.[1] It contains a C-terminal CAAX box (where C is cysteine, A an aliphatic amino acid, and X any amino acid), which is farnesylated in vivo and localizes PRL-3 to inner membranes, particularly the plasma membrane and early endosome.[1] This is a unique feature among PTPs; however, it is a common feature among inositol phosphatases.[6] One of the DSPs structurally most similar to PRL-3 is PTEN,[7]

and the sequence homology between the two (Figure 1) has already been recognized in early molecular cloning studies.[8] PTEN is a DSP with activity toward 3-phosphorylated PIPs, particularly $PI(3,4,5)P_3$.[9] Studies in cell lines that stably express ectopic PRL-3 prove a direct correlation between elevated PRL-3 levels and the acquisition of a migratory and invasive phenotype.[1,2] However, until now, the underlying biochemical mechanisms are still widely unknown.[1,2] So far, only a limited number of proteins have been suggested as natural substrates: Ezrin,[10,11] Keratin 8,[12] Integrinβ1,[13,14] and Stathmin.[15] Integrinα1 has been described as a direct interaction partner of PRL-3.[13] PRL-3 has been reported to regulate Rho family GTPases[16,17] and to be involved in downregulating Csk (C-terminal Src kinase) leading to Src kinase activation[18] via eIF2 using a general mechanism of inhibition of protein trans-

```
hPRL-3     1 ----------MARMN------RPAPVEVSYKHMRFLITHNPTNA----T--LSTFIE  35
hPTEN      1 MTAIIKEIVSRNKRRYQEDGFDLDLTYIY---PNIIAMGFPAERLEGVYRNN---ID  51
hPRL-3
hPTEN

hPRL-3    36 DLKKYG--ATTVVRVCE-----VTYDKTPLEKDGITVVDWPFD-DGAPPPGKVVEDW  84
hPTEN     52 DVVRFLDSKHKNHYKIYNLCAE----RHYDTAKFNCRVAQYPFEDNPPQLELIKPF 104
hPRL-3
hPTEN

hPRL-3    85 LSLVKAKFCEAPGSCVAVHCVAGLGRAPVLVALALI-ESG-MKYEDAIQFIRQKR-- 137
hPTEN    105 CEDLDQWLSEDDNHVAAIHCKAGKGRTGVMICAYLLHRGKFLKAQEALDFYGEVRTR 161
hPRL-3
hPTEN

hPRL-3   138 --RGAINSKQLTYLEKYRPKQRLR----FKDPHTHKTRCCVM                173
hPTEN    162 DKKGVTIPSQRRYVYYYSYLLKNHLDYRPVALLFHK-----                 197
hPRL-3
hPTEN
```
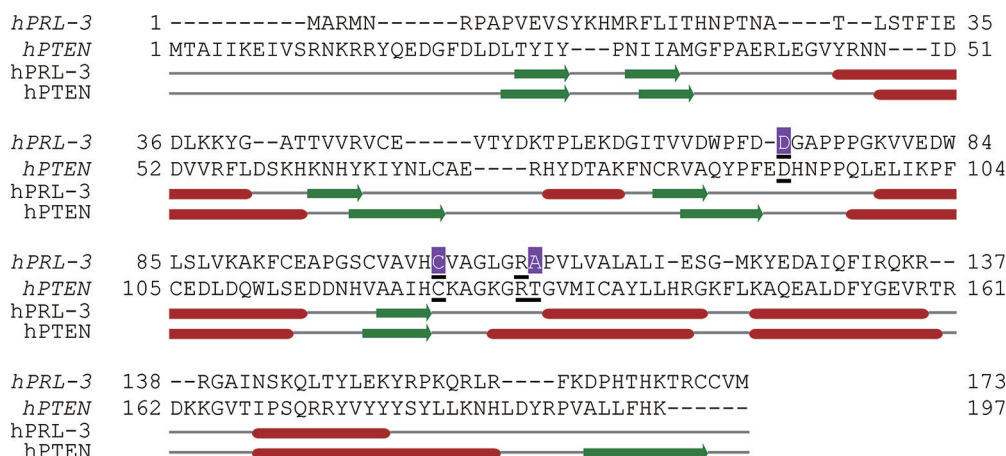
Figure 1. Sequence and structural alignment of PRL-3 with PTEN.[21] The mutated residues in PRL-3 used in this study are colored purple (D72, C104, and A111). Catalytic residues are underlined. Secondary structures are labeled according to PDB entries 1V3A and 1D5R (α-helix, red band; β-sheet, green arrow).

lation.[19] PRL-3 activity in cancer has also been linked to the PTEN-PI3K pathway potentially as an upstream posttranscriptional negative regulator of PTEN translation to promote epithelial-mesenchymal transition (EMT).[16] In addition, PRL-3 has been shown to promote EMT by direct regulation of Cadherin.[20] Unfortunately, the suggested substrates have so far not been placed into direct context with the pathways affected by PRL-3. Because PRL-3's natural substrates remain unclear and the enzyme so far could not be placed conclusively into any signaling pathway, we sought to map PRL-3's substrate specificity in vitro and to investigate the structure–activity relationship of PRL-3 toward potential substrates by investigating key PRL-3 variants. Thereby, we analyzed wild-type (WT) PRL-3 and three PRL-3 variants known to affect the catalytic activity of the enzyme: C104S, D72A, and A111S (Figure 1).

First, the phosphatase activity of these variants was compared using OMFP as a substrate,[21] and far-UV circular dichroism (CD) spectra were acquired, including melting temperatures, to analyze the secondary structure of the variants.[22] The PRL-3 variants were then further characterized with respect to their phosphatase activity toward phosphopeptides and phosphoinositides. The chosen peptides were designed on the basis of proteins reported to be potential natural substrates. PRL-3 did not show any significant activity toward the phosphopeptides. Phosphoinositide activity for PRL-3 has not yet been reported.[23] We discovered that PRL-3 dephosphorylates PI(4,5)P$_2$ and, to a lesser extent, PI(3,4,5)P$_3$ in vitro. Our data, including dephosphorylation assays and molecular modeling, suggest that PRL-3 is a phosphatidylinositol 5-phosphatase. Subsequently, the cellular phenotype of WT PRL-3 and the variants with respect to promoting cell migration in a wound healing assay was investigated using stably transfected HEK293 cell lines. The cellular phenotype that we observed correlates well with the structure–activity analysis of all variants and the WT protein. Thus, we can suggest that PRL-3's role in cell migration can be related to its ability to dephosphorylate PI(4,5)P$_2$ or PI(3,4,5)P$_3$.

■ MATERIALS AND METHODS

Materials. Fmoc-protected amino acids HBTU, HOBt, and Rink amide resin were purchased from Calbiochem. DMF,

piperidine, and DCM were purchased from VWR. Glutathione S-transferase (GSTrap FF, 1 mL) and NiNTA purification columns were purchased from Amersham Biosciences/GE Life Science. Protease inhibitor cocktail tablets were purchased from Roche. The EnzChek phosphatase assay kit was purchased from Molecular Probes. All soluble di-C8-D-myophosphatidylinositol phosphates were purchased from Echelon Biosciences. All other reagents were purchased from Sigma-Aldrich.

Bacterial Strains and Plasmid Vectors. Plasmid vector pET15b was used to overexpress recombinant human WT and mutant PRL-3 forms as His-tagged fusion proteins, and vector T7-7 was used to overexpress human His-tagged PTP1B. Human PTEN and human type IV 5-phosphatase (5-ptase) were overexpressed as GST-tagged fusion proteins using pGEX-4T-1 and pBADM-30, respectively, as vectors. All recombinant proteins were transformed into *Escherichia coli* strain BL21 DE3 using standard methods that have been previously described.[24] Bacterial cultures were grown at 37 °C with shaking, and protein expression was induced with 0.1 mM IPTG for PRL-3 variants and PTEN and 0.2% arabinose for 5-ptase. Proteins were induced for 3 h at 37 °C.

Construction of Mutant PRL-3 Proteins. A111S PRL-3, C104S PRL-3, and D72A PRL-3 proteins were constructed using single-step polymerase chain reaction using complementary primers encoding the codon change. Primers 5′ ggcctgggccggtctccagtccttg 3′ and 5′ caaggactggagaccggcccaggcc 3′ were used to construct A111S. Primers 5′ cgtttgacgctggggcgcc 3′ and 5′ ggcgccccagcgtcaaacg 3′ were used to construct D72A. Primers 5′ ctgtgcactccgtggcgggg 3′ and 5′ cccgccacggagtgcacag 3′ were used to construct C104S. Mutant constructs were confirmed by DNA sequencing.

Expression and Purification of Recombinant Proteins. BL21 DE3 cells expressing the recombinant WT and mutant forms of PRL-3 were lysed by sonication in buffer A [50 mM Tris-HCl (pH 7.4) containing 500 mM NaCl, 20 mM imidazole, 1 mM dithiothreitol (DTT), and 0.5 mM protease inhibitor cocktail]. The proteins were purified using a FPLC Histrap HP 1 mL column using an elution gradient from 20 to 500 mM imidazole in buffer A. The purified PRL-3 proteins were dialyzed against 50 mM Tris-HCl (pH 7.4), 150 mM NaCl, 5 mM DTT, and 10% glycerol. BL21 DE3 cells expressing the recombinant His-PTP1B were lysed by

sonication in lysis buffer [20 mM Tris-HCl (pH 8.0) containing 150 mM NaCl, 10 mM imidazole, 1 mM DTT, and 0.5 mM phenylmethanesulfonyl fluoride (PMSF)]. The protein was purified using a FPLC Histrap HP 1 mL column using an elution gradient from 10 to 500 mM imidazole in buffer A. BL21 DE3 cells expressing recombinant GST−PTEN fusion protein were lysed in 50 mM Tris-HCl (pH 8.0), 250 mM NaCl, and 0.5 mM protease inhibitor cocktail. The cell lysate was applied to a FPLC GSTrap FF 1 mL column; the column was washed with 50 mM Tris-HCl (pH 8.0) and 50 mM NaCl, and then the GST−PTEN fusion protein was eluted with 50 mM Tris-HCl (pH 8.0), 50 mM NaCl, and 10 mM glutathione. Purified GST−PTEN fusion protein was dialyzed against 50 mM Tris-HCl (pH 8.0), 150 mM NaCl, and 1 mM DTT. BL21 DE3 cells overexpressing the pBADM-30-GST-5-ptase were lysed in 50 mM sodium phosphate (pH 6.8), 200 mM NaCl, 2 mM DTT, 0.1 mg/mL lysozyme, and 0.5 mM protease inhibitor cocktail, using a French press, with four passes. The cell lysate was applied to a FPLC GSTrap FF 1 mL column, and the column was washed with 50 mM sodium phosphate (pH 6.8), 50 mM NaCl, 2 mM DTT, and 0.5 mM protease inhibitor cocktail. Then the GST−5-ptase fusion protein was eluted with 50 mM sodium phosphate (pH 6.8), 50 mM NaCl, 2 mM DTT, and 10 mM glutathione. The integrity of all proteins was confirmed by molecular weight determination by electrospray ionization mass spectroscopy (ESI-MS).

Peptide Synthesis. Peptides were synthesized on solid phase Rink amide resin by standard coupling and Fmoc protection strategies using an automated MultiSynTech peptide synthesizer. Peptides were isolated after cleavage from resin and deprotection using 95 vol % trifluoroacetic acid and 5 vol % triisopropylsilane. The peptides were ether-precipitated and purified to homogeneity (>90% purity) using high-performance liquid chromatography, and identities were confirmed by ESI-MS.

Far-UV Circular Dichroism (CD). WT PRL-3 and mutant variants were dialyzed into 20 mM Tris-HCl (pH 7.4), 50 mM NaCl, and 1 mM DTT. Protein concentrations after dialysis were determined by absorption at 280 nm using a NanoDrop spectrophotometer. The concentrations used in the CD measurements were 0.48 mg/mL for WT PRL-3, 0.43 mg/mL for the D72A mutant, 0.64 mg/mL for the A111S mutant, and 0.6 mg/mL for the C104S mutant. Far-UV CD spectra were recorded using a Jasco J-715 spectropolarimeter. The spectropolarimeter was purged with N_2 for 15 min prior to measurement. CD was measured over the far-UV range (195−250 nm) at 20 °C using a path length of 0.1 cm. The scan speed was set to 10 nm/min with a wavelength interval of 1 nm. Four or five scans were acquired and automatically averaged. The far-UV signal over the entire range was initially measured using a buffer sample in the absence of enzyme to determine the baseline for subsequent CD spectra. Far-UV CD spectra were acquired for WT PRL-3 and for the variants in duplicate. The spectra were then averaged and buffer subtracted as well as normalized to a protein concentration of 1 mg/mL. The thermal stability of the PRL-3 proteins was also compared by monitoring the CD signal at 223 nm as a function of temperature over a range of 20−85 °C with intervals of 0.2 °C. The sample was cooled in the spectropolarimeter, and observation of the CD signal upon cooling showed that the thermal denaturation of WT PRL-3 and the variants was irreversible. Therefore, thermodynamic parameters could not

be quantitatively determined from the CD data. The midpoint of the thermal denaturation curve was estimated and used as a qualitative comparison of the stability of the different proteins.

Phosphatase Activity Assays. A standard enzymatic activity assay was conducted using 3-O-methylfluorescein phosphate (OMFP) as a substrate. The assay was conducted at 37 °C in 40 mM Tris-HCl (pH 6.2), 150 mM NaCl, and 4 mM DTT. WT PRL-3 and mutant variants were assayed at 6 μM. OMFP was used at 600 μM in all reactions. The assay was conducted in 96-well plate format and monitored by absorbance at 450 nm over time. The release of phosphate from candidate peptide and lipid substrates was monitored using a commercially available phosphatase assay kit, EnzChek, according to the manufacturer's instructions. WT PRL-3 and mutant variants [2 μM, 4.5 μM (for phosphopeptide activity assays), or 6 μM (for PIP activity assays)] were incubated with 50 mM Tris-HCl (pH 7.5), 150 mM NaCl, 1 mM $MgCl_2$, and 4 mM DTT in 96-well plates with either 100 μM phosphopeptide or 100 μM phosphoinositide substrates. The assay was conducted at 37 °C with shaking in a Tecan Safire TM plate reader. The release of phosphate from the candidate substrates was continually monitored by measuring absorbance at 360 nm. For the controls, 52 nM PTP1B was incubated with 50 μM phosphopeptide substrate, and 0.9 μM PTEN and 5.8 μM 5-ptase were incubated with 100 μM phosphoinositide in the same buffer used for the PRL-3 measurements. Assays conducted in the absence of enzyme were included in the 96-well plate setup in triplicate for all the substrates analyzed. The measurements in the absence of enzyme were averaged and subtracted from the data to account for nonspecific hydrolysis of the substrates and for background absorption. The data were normalized toward the signal of $PI(3,4,5)P_3$ in the no enzyme control to account for potential differences due to the use of multiple plates. In all phosphatase assays, the measurements were taken in triplicate and the standard deviation of the measurements is represented as error bars. Data were plotted using SigmaPlot11.

Dephosphorylation assays of fluorescently labeled PIPs (Echelon Biosciences) were conducted using recombinant PRL-3 (4.5 or 9 μg) in 20 μL of reaction buffer containing 50 mM MES (pH 6.5) and 1 mM TCEP [tris(2-carboxyethyl)-phosphine] with 1.0 μg of fluorescent di-C6-NBD6 or fluorescent di-C6-BODIPY phosphoinositide substrates for 1 h at 37 °C. Phosphatase assays using recombinant PTEN were conducted in 20 μL of reaction buffer containing 50 mM ammonium carbonate (pH 8.0) in the presence of 1 mM TCEP. Phosphatase assays using recombinant 5-ptase were conducted in 20 μL of reaction buffer containing 50 mM Tris-HCl (pH 7.5), 50 mM NaCl, and 3 mM $MgCl_2$. Phosphatase reactions were terminated by addition of 100 μL of acetone and then mixtures evaporated to dryness in a Speed-Vac evaporator. The dried reaction products were resuspended in 20 μL of a methanol/chloroform mixture (1/1) and spotted onto a glass-backed TLC plate (HPTLC Silica gel 60, 10 cm × 10 cm, Merck).[25] The TLC plate was developed in a chloroform/acetone/methanol/glacial acetic acid/water solvent system (80/30/26/24/14) as described previously and air-dried.[25] Fluorescent lipids were visualized using a model FLA 7000 Fuji Bio-Imaging System.

Phosphatase assays using immunoprecipitated FLAG-tagged PRL-3 wild-type, C104S, D72A, or A111S proteins were conducted by incubating resin-bound proteins for 1 h at 37 °C

in 30 μL of reaction buffer (above) containing 1 μg of di-C6-NBD6-phosphatidylinositol 4,5-diphosphate. The samples were then centrifuged for 30 s to pellet the beads, and 20 μL of supernatant was removed. Acetone (100 μL) was added to each supernatant, and the samples were dried and analyzed as described above.

Molecular Modeling. The PRL-3 structure in the "closed" active conformation was obtained via homology modeling using the crystal structure of PRL-1 (C104S) in complex with a sulfate ion (PDB entry 1XM2)[26] as a template. Homologue proteins of human PRL-3 were identified from UniProt,[27] and ClustalW2[28] was used for multiple-sequence alignment. The alignment result between PRL-3 (Q75365) and PDB entry 1XM2 coincides with those in previous studies.[26,29] MODELER (Release 9v8)[30] was then used for homology modeling. The sulfate ion was kept in the active site during model generation. Eleven models were generated, and the best model was selected by three criteria: "normalized DOPE score" (MODELER), "dfire_energy" (DFire),[31] and "model quality score" (ModFOLD).[32] This model was further refined by MD simulation using NAMD (version 2.7b4)[33] with an Amber force field. The charges and force field parameters of the sulfate ion were obtained using the Antechamber[34] module in AMBER-Tools (version 1.4), where the charge models were calculated via the AM1-BCC method. Atoms on PRL-3 were assigned the parameters of the ff03 force field. The PRL-3−sulfate complex was soaked in a box of TIP3P[35] water molecules with a margin of 10 Å along each dimension. Chloride ions were added to neutralize the whole system. The system was first minimized with restraints of 5.0 kcal/mol on protein and sulfate ion for 5000 steps. The time step size was set to 2 fs. Then, the system was further minimized without constraints for 15000 steps. After that, a 62 ps simulation was used to gradually increase the temperature of the system from 0 to 310 K. A subsequent 500 ps simulation was performed to equilibrium under a constant temperature of 310 K and a constant pressure of 1 atm. The nonbonded cutoff distance was set to 12 Å. During the entire MD simulation, Cys-104 was treated as the deprotonated form while Asp-72 was treated as the protonated form. The last snapshot of the MD simulation was selected as the final PRL-3 model.

The three-dimensional (3D) structural model of diC8-PI(4,5)P_2 (the deprotonated form) was built on the basis of PI(3)P, which was extracted from PDB entry 1ZSQ.[36] It was further optimized via OpenBabel (version 2.2.3)[37] using the MMFF94 force field. GOLD (version 5.0.1, CCDC Software)[38] was then used in molecular docking of diC8-PI(4,5)P_2 to the PRL-3 model. GoldScore was selected as fitness function and automatic (ligand-dependent) genetic algorithm parameter settings were used with the search efficiency set to 100%. The active site residues Arg-6, Asp-72, Val-105, Leu-108, Arg-110, and Arg-138 were treated as flexible during docking. For the constrained docking study, the 4- or 5-phosphate group of diC8-PI(4,5)P_2 was constrained to point into the catalytic site during docking by setting the constraints for the H−O distance between Asp-72 COOH and O-PO3-diC8-PI(4,5)P_2 (1.6−2.0 Å) and the S−P distance between Cys-104 S and P-O4-diC8-PI(4,5)P_2 (3.0−3.8 Å).

Generation of Cell Lines Stably Expressing PRL-3 Variants. The Flp-In 293 T-Rex (tetracycline-regulated system) cell line (Invitrogen) was used to create isogenic cell lines stably expressing wild-type and mutant PRL-3 proteins with N-terminal FLAG epitope tags. Cells were grown in Dulbecco's modified Eagle's medium (DMEM) supplemented with 1% glutamine, 1% penicillin/streptomycin, 10% fetal bovine serum (FBS) (Invitrogen), 15 μg/mL of blasticidin, and 100 μg/mL hygromicin. The expression of the PRL-3 proteins was induced by addition of 1 μg/mL tetracycline to the growth medium.

Western Blot. Cell lysates were subjected to sodium dodecyl sulfate−polyacrylamide gel electrophoresis (SDS−PAGE) and immunoblot analysis with antibodies against FLAG (Sigma) and β-actin (Sigma).

Indirect Immunofluorescence. To visualize FLAG-tagged PRL-3, HEK293 cells stably expressing either WT PRL-3 or mutants were seeded onto LabTek eight-well chamber slides (NUNC) precoated with polylysine. Cells were fixed with 4% paraformaldehyde for 15 min at room temperature, permeabilized with 0.1% Triton X-100 and phosphate-buffered saline for 10 min, and blocked with 1% bovine serum albumin for 1 h. The anti-FLAG antibody was then added to the cells, followed by the Alexa Fluor 488 goat anti-mouse IgG secondary antibody (Invitrogen). After being washed with phosphate-buffered saline, cells were incubated with Hoechst 33342 (2 μg/mL) for 5 min and imaged using a Leica SP2 sirius confocal microscope system.

Wound Healing Motility Assays. Cell migration assays were conducted using μ-Dish 35 mm Culture Inserts (Ibidi) according to the manufacturer's protocols. In brief, cells stably expressing either PRL-3 wild-type, mutants, or an empty vector were seeded into each well of the culture inserts in the presence of tetracycline and incubated at 37 °C in a humidified atmosphere with 5% CO_2. On the day of experimentation, the culture inserts were gently removed by using sterile tweezers, and the dish was filled with fresh DMEM supplemented with 5% FBS. Photos of the wound were taken under a Zeiss Cellobserver HS microscope (10× magnitude).

Immunoprecipitation of PRL-3 Proteins. Cells stably expressing PRL-3 proteins were grown in the presence of tetracycline. Cells were lysed on ice in a buffer containing 50 mM Tris-HCl (pH 7.4), 150 mM NaCl, 1 mM EDTA, and Complete Protease Inhibitor (Roche) by being passed through 26-gauge needles 10 times. Lysates were cleared by centrifugation (10 min at 18000g and 4 °C), and the supernatants were incubated on a rocker for 2 h at 4 °C with 40 μL of anti-FLAG M2-agarose affinity resin (Sigma). Samples were washed three times with lysis buffer followed by an additional wash with the phosphatase reaction buffer (see above).

■ RESULTS AND DISCUSSION

Characterization of the PRL-3 Variants. To characterize the in vitro phosphatase activity of PRL-3, we analyzed wild-type (WT) PRL-3 and three key variants, C104S, D72A, and A111S PRL-3. Mutation of the essential active site Cys 104 to Ser inactivates PRL-3 phosphatase activity.[10] In the D72A mutant, the activity of PRL-3 is also affected by the disruption of the acidic loop that is required for hydrolysis of a substrate once it is bound to the active site, and the mutant has been reported to be catalytically inactive, at least toward OMFP.[21] With regard to the A111S mutant, an active site Ser residue is a conserved feature among many DSPs and is implicated in the catalytic mechanism. Such a Ser is not featured in the PRL family of DSPs, possibly explaining the much weaker in vitro

activity of PRLs relative to those of other DSPs. The variant of PRL-3 in which Ala 111 has been substituted with Ser has been reported to be hyperactive toward OMFP.[21] The phosphatase activity of the proteins was initially compared using OMFP as a substrate[21] (Figure 2). Consistent with a previous report,[21] WT
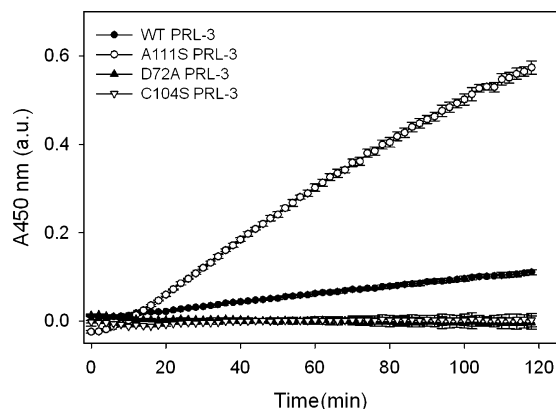

Figure 2. Hydrolysis of OMFP (600 μM) by wild-type PRL-3 and mutant forms of PRL-3: A111S, D72A, and C104S (6 μM each). Measurements were taken in triplicate, and the standard deviation of the measurements is represented as error bars.

PRL-3 exhibits very weak activity toward OMFP, D72A PRL-3 shows no significant dephosphorylation of OMFP, and the A111S mutant exhibits considerably higher activity than WT PRL-3. Mutation of the essential active site Cys 104 to Ser inactivates PRL-3 phosphatase activity.

To further characterize WT PRL-3 and its variants, far-UV circular dichroism (CD) spectra were acquired.[22] The CD measurements show significant structural changes for the A111S and C104S mutants compared to WT PRL-3, whereas D72A exhibited much less structural perturbation (Figure 3A). The CD signal was then monitored at increasing temperatures to compare the thermal stability of the PRL-3 variants. The apparent melting temperatures of C104S (52 $\pm$ 2 °C) and A111S (51 $\pm$ 2 °C) are significantly lower than that of WT PRL-3 (62 $\pm$ 2 °C), while the melting temperature of D72A appears to be higher [>65 °C (Figure 3B–E)]. These results suggest that the mutations within the catalytic region of PRL-3, i.e., the A111S and C104S mutations, have a more significant impact on the structural stability of PRL-3 than a mutation in a distant region (D72A). In both destabilized variants, a hydrophilic residue is introduced into the hydrophobic p-loop of PRL-3.[39] This could also contribute to the structural destabilization.

Determination of the Catalytic Activity and Specificity of WT PRL-3 and Its Variants. The phosphatase activity of WT PRL-3 and A111S PRL-3 toward phosphorylated peptide substrates was then analyzed. The A111S mutant was used because of its enhanced activity toward OMFP and thus potential higher sensitivity. The phosphatase concentrations were chosen to be in the low micromolar range, and thus quite high, because of the reported low activity of PRL-3 toward peptides and OMFP in vitro,[21] and for the same reason, a high peptide concentration was selected (100 μM). A commercially available dephosphorylation assay (EnzChek) was used to monitor the release of phosphate continuously over time (Figure 4, data at 30 min). The peptide substrates [peptides 1–

6 (Table 1)] were designed on the basis of proteins reported to be affected by PRL-3 and thus potentially interact with PRL-3 in vivo.[7,10,11,13,14,16–18] Three more peptides [peptides 7–9 (Table 1)] were included to increase the variety of amino acid properties and peptide length.

Neither WT PRL-3 nor A111S PRL-3 dephosphorylates any of our peptide substrates significantly (Figure 4). As a positive control, dephosphorylation of peptides by the Tyr-specific phosphatase PTP1B[40] was monitored in parallel with PRL-3. PTP1B shows a high degree of phosphatase activity toward phosphotyrosine peptides. Because of the potential further application of the peptides, they were either biotinylated or acetylated. Comparison between peptides 1 and 2 shows that the addition of either group has no effect on PRL-3 phosphatase activity. The lack of in vitro activity of PRL-3 toward phosphopeptides could indicate that PRL-3 needs a cofactor or post-translational modification to be able to dephosphorylate proteins, or that it requires the entire protein for recognition as a substrate. On the other hand, other DSPs such as CDC25 and MKP3 have also been reported to have weak activity toward peptides derived from protein substrates;[41,42] thus, the lack of in vitro activity is not necessarily unusual.

PRL-3 is structurally similar with the lipid phosphatase PTEN (Figure 1), and it carries a C-terminal CAAX box, which not only is featured in known lipid phosphatases but also localizes PRL-3 to the cellular compartments rich in phosphoinositides (PIPs). In addition, certain PIPs such as PI(3,4,5)P_3 and PI(3,4)P_2 and also depletion of PI(4,5)P_2 have been described as being involved in promoting cell motility, and these roles have been shown to be important in cancer.[43] Thus, further investigations were conducted using PIPs as lipid substrates. The release of phosphate from soluble PIP substrates carrying dioctanoyl (diC8) lipid chains by WT, C104S, D72A, and A111S PRL-3 as well as PTEN and type IV 5-phosphatase (5-ptase) was continuously measured over 2 h using the EnzChek assay. 5-ptase does not belong to the PTP superfamily and uses a catalytic mechanism different from that of PTPs; however, it has been reported to dephosphorylate PI(4,5)P_2 and PI(3,4,5)P_3[44] and was therefore used here as a second control. The signal intensity after dephosphorylation for 30 min was used to compare the substrate preferences of each individual enzyme against the whole range of phosphoinositides. The resulting substrate preference profiles are shown in Figure 5A.

As expected, PTEN dephosphorylates PI(3,4,5)P_3 and shows no significant activity toward the other PIPs (Figure 5A). Also as expected, 5-ptase removes phosphate preferentially from PI(4,5)P_2 and PI(3,4,5)P_3, demonstrating the robustness of the assay. WT PRL-3 exhibits lipid phosphatase activity toward PI(4,5)P_2 and, to a lesser extent, toward PI(3,4,5)P_3, with no significant activity measured against the other PIP substrates. D72A PRL-3 shows weakened lipid phosphatase activity but with the same substrate preferences as WT PRL3. The C104S and, surprisingly, A111S variants exhibit no lipid phosphatase activity toward any of the measured phosphoinositide substrates.

By comparison of the substrate preference profiles of all the phosphatases assayed here (Figure 5A), it is clear that WT PRL-3 and the less active D72A variant show substrate preferences very similar to those of 5-ptase, rather than those of PTEN. Although the substrate preferences of PRL-3 match
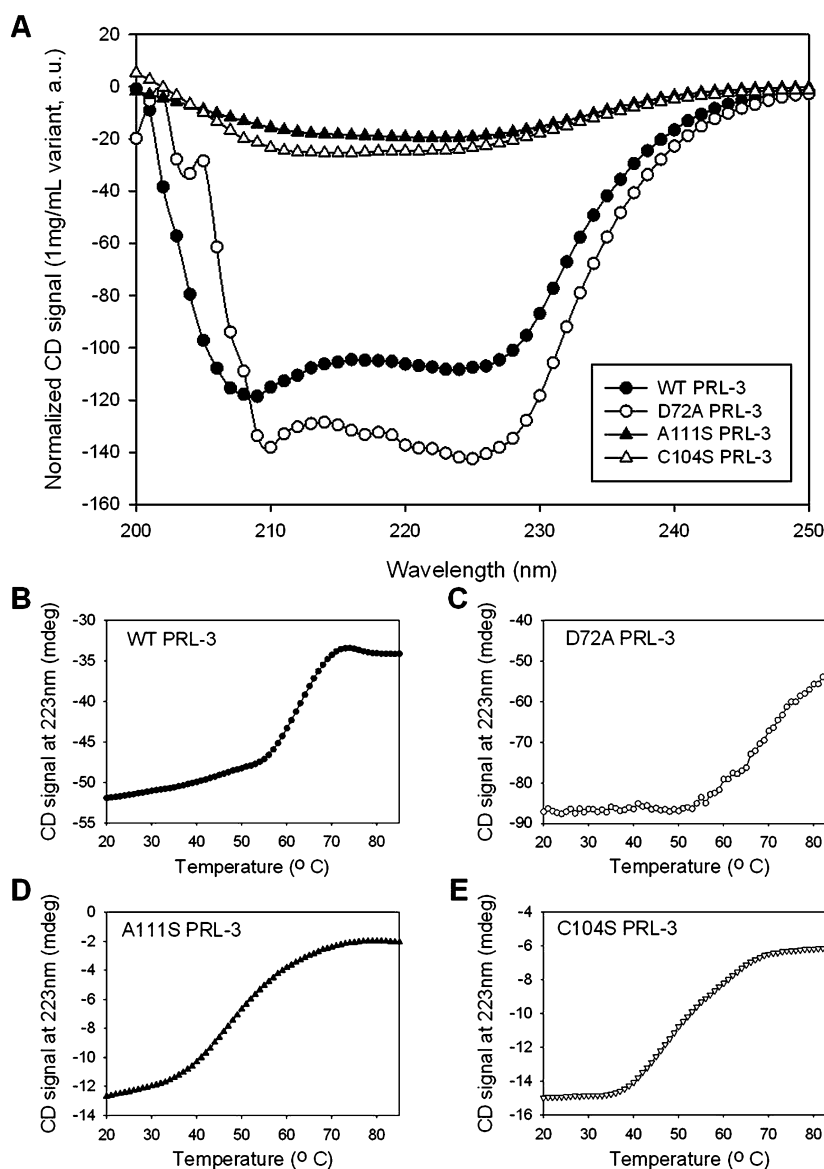
Figure 3. Secondary structure analysis of the PRL-3 variants by far-UV CD. (A) Far-UV CD spectra of WT PRL-3 as well as the D72A, C104S, and A111S mutants. (B−E) Thermal stability curves of WT PRL-3 (B), D72A PRL-3 (C), A111S PRL-3 (D), and C104S PRL-3 (E). For experimental details, see Materials and Methods.

those of the 5-ptase and partially match those of PTEN, there are significant differences in the kinetics of dephosphorylation for each of these enzymes. Dephosphorylation of PI(3,4,5)P3 by PRL-3 compared to that by PTEN and 5-ptase is shown in Figure 5B. In spite of the lower concentration used in our assay, PTEN is more active than PRL-3 toward PI(3,4,5)P3. The 5-ptase, assayed here at high concentrations like those of PRL-3, also has faster activity against PI(3,4,5)P3 than PRL-3. The dephosphorylation of PI(4,5)P2 by PRL-3 and 5-ptase is compared in Figure 5C. These kinetic traces clearly show that 5-ptase demonstrates faster reaction kinetics toward PI(4,5)P2 than PRL-3.

The D72A and A111S PRL-3 variants show discrepancies between their activities toward OMFP and toward PIPs. The D72A variant has no activity against OMFP but does have attenuated wild-type-like activity toward the PIP substrates (Figures 2 and 5A). This could be simply due to enhanced sensitivity to the PIPs as potential natural substrates compared to the unnatural OMFP substrate, or because of the apparent

overall structural stabilization of the mutant as indicated by our CD studies. In addition, D to A mutant PTPs have been reported to be able to sustain some catalytic activity, presuming another residue in the protein can substitute the missing general acid required for the catalytic mechanism.[45] Within the active site of PTPs, there is a conserved Ser/Thr that could fulfill this role.[45] However, there is no such equivalent residue in the active site of PRL-3 (A111), indicating that the general acid property needs to be provided by another residue within the protein or from the substrate itself. The highly negatively charged PIPs as substrates for PRL-3 could quite feasibly compensate for the loss of acid in the mechanism of dephosphorylation by the D72A mutant. The A111S PRL-3 variant has been shown to be a hyperactive form of the protein toward OMFP[21] (Figure 2), yet this mutant does not dephosphorylate any PIP substrates in our in vitro assays (Figure 5A). Given that our CD studies show perturbations in the structure of A111S PRL-3 relative to that of the wild-type protein, this Ala residue could play an important role in
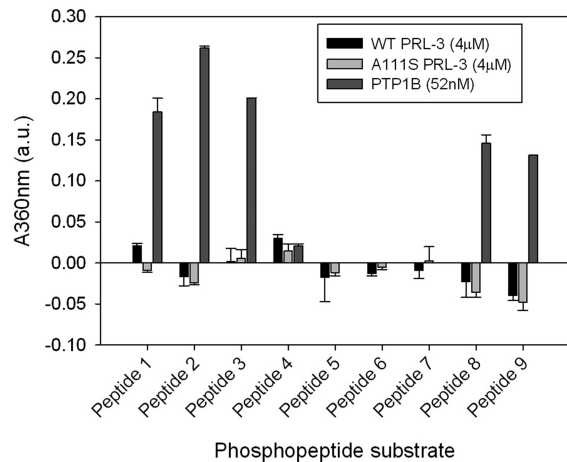
Figure 4. Dephosphorylation of phosphopeptides by WT PRL-3 (4 μM, black), A111S PRL-3 (4 μM, light gray), and PTP1B (52 nM, dark gray). Phosphopeptides were assayed at 100 μM for PRL-3 variants and at 50 μM for PTP1B. Phosphate release was measured in triplicate using the EnzChek assay (see Materials and Methods). The averaged data are shown, and the standard deviation is represented as error bars. Absorption intensities of <0.05 au are considered to be not significant because of combined spectral and manual error.

Table 1. Sequence Features and Origins of the Phosphorylated Peptides Used as Substrates for in Vitro Dephosphorylation Assays

entry	sequence[a]	protein origin	phospho site
1	biotin-GENPIpYKSAV-NH$_2$	Integrinβ1	Y783[b]
2	Ac-GENPIpYKSAV-NH$_2$	Integrinβ1	Y783[b]
3	biotin-VVNPKpYEGK-NH$_2$	Integrinβ1	Y795[b]
4	biotin-QGRDKYKpTLRQIRQG-NH$_2$	Ezrin	T567[c]
5	biotin-ASSSTSVpTPDVSDNEPDHY-NH$_2$	PTEN	T366[b]
6	Ac-IpSPPPTANL-NH$_2$	FAK1	S910[b]
7	Ac-IQAAApSTP-NH$_2$	GSK3β	S389[b]
8	Ac-DpYpYR-NH$_2$	IR	Y1189, Y1190[b]
9	Ac-DKEpYpYKVKEPGES-NH$_2$	JAK2	Y1007, Y1008[b]

[a]NH$_2$ is the C-terminal amide; Ac is the N-terminal acetyl group, and biotin denotes N-terminal biotinylation. [b]UniProt data. [c]From refs 10 and 11.

maintaining the integrity of the active site. However, on the basis of our current data, we cannot determine unequivocally whether the inactivity of A111S PRL-3 and the activity of D72A PRL-3 toward PIP substrates are due to structural changes relative to the WT protein or differences in the enzymatic mechanism. For C104S PRL-3, the lipid phosphatase activity is consistent with the OMFP activity assays, which demonstrates that replacing Cys 104 with Ser completely inactivates the phosphatase.

To further validate our findings, we repeated the dephosphorylation assay with PI(4,5)P$_2$ and PI(3,4,5)P$_3$ using PIP derivatives that are fluorescently labeled in one lipid chain. The dephosphorylation of the substrates was analyzed by thin layer chromatography (Figure 6). As seen in Figure 6A, PI(4,5)P$_2$ is dephosphorylated by PRL-3 and 5-
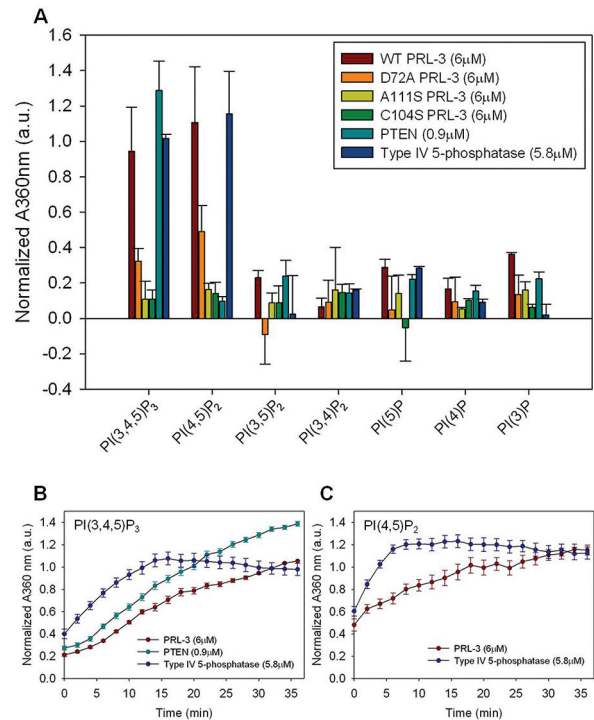

Figure 5. Dephosphorylation of PIPs by WT PRL-3 and its variants (6 μM), PTEN (0.9 μM), and type IV 5-phosphatase (5.8 μM). The full range of phosphoinositide substrates was analyzed at 100 μM. (A) The absorption at 360 nm after dephosphorylation of each substrate for 30 min shows the substrate preference profiles for each enzyme. (B and C) Kinetic traces of dephosphorylation of (B) PI(3,4,5)P$_3$ by WT PRL-3, PTEN, and type IV 5-phosphatase and (C) PI(4,5)P$_2$ by WT PRL-3 and type IV 5-phosphatase. Measurements were taken in triplicate and individually corrected for background by subtracting the absorbance from a corresponding PIP sample incubated in the absence of enzyme. The background-corrected absorbance was then normalized to the signal of the PI(3,4,5)P$_3$ control without enzyme and averaged. The standard deviation of the averaged normalized data is represented as error bars. Absorption intensities below 0.30 au (resulting from normalization of the original value of 0.05 au and averaging) are considered to be not significant because of the combined spectral and manual error.

ptase but not PTEN, confirming the results of the previous assay. Dephosphorylation of PI(3,4,5)P$_3$ by WT PRL-3 was not seen in this assay; it was, however, dephosphorylated by PTEN and 5-ptase, showing the robustness of this assay (Figure 6B).

It is unclear why PRL-3 lacks PI(3,4,5)P$_3$ phosphatase activity in this assay. We can speculate that the different result could be due to the presence of a different lipid chain in the fluorescent PIP; however, this was not represented in the PI(4,5)P$_2$ data. Also, the weak in vitro activity of PRL-3 could contribute to this result. Despite such discrepancies, we have definitively confirmed PRL-3 phosphatase activity toward PI(4,5)P$_2$, and thus, PRL-3 could be the first phosphatase in the PTP superfamily to dephosphorylate this PIP.

We then analyzed the product of PI(4,5)P$_2$ dephosphorylation by PRL-3 by comparing the product to the monophosphorylated PIPs to determine which phosphate on the ring is released by PRL-3. Figure 7 shows the fluorescence read-out of the dephosphorylation of PI(4,5)P$_2$, PI(4)P, and PI(5)P by PRL-3. The monophosphorylated PIPs run quite close. PI(4)P runs closer to the product of the PI(4,5)P$_2$ dephosphorylation
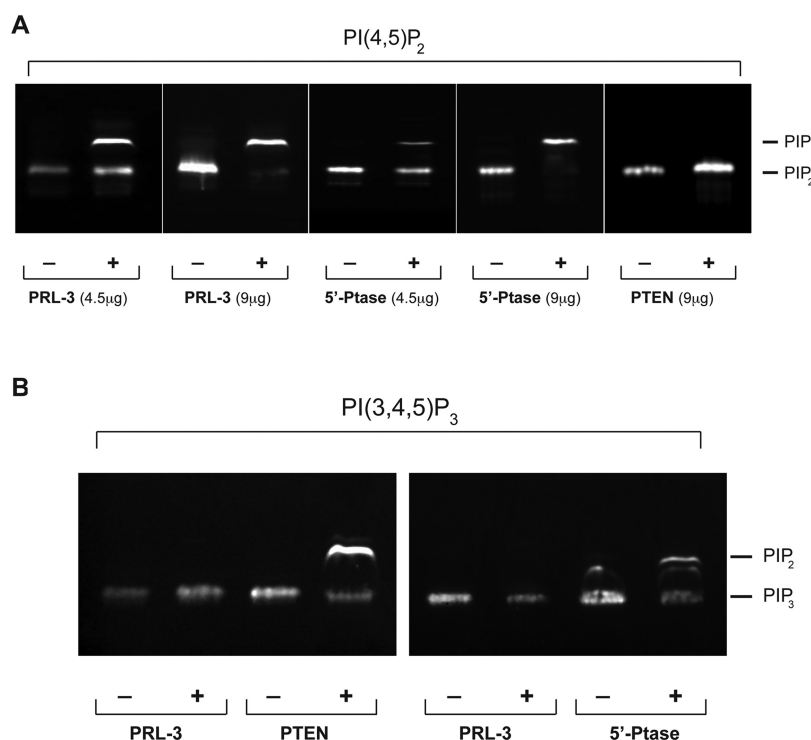
Figure 6. Dephosphorylation of fluorescently labeled $PI(4,5)P_2$ (A) and $PI(3,4,5)P_3$ (B) by WT PRL-3, 5-ptase, and PTEN. Phosphatase assays containing 1.0 μg of fluorescent phosphoinositide substrate were conducted for 1 h at 37 °C with buffer (−) or with different concentrations of recombinant proteins (as indicated), processed as described in Materials and Methods, and analyzed by TLC. $PI(3,4,5)P_3$ dephosphorylation assays were performed under the same conditions using 9 μg of recombinant protein. Shown is a representative result of three experiments.
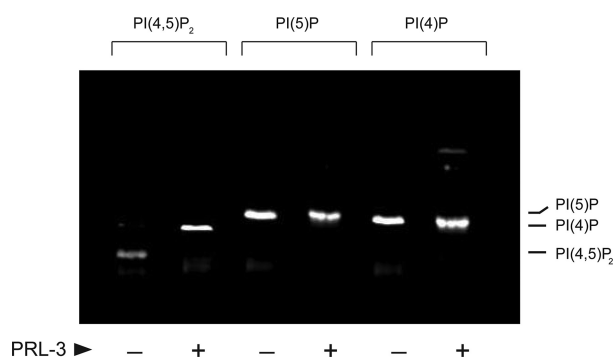
Figure 7. Dephosphorylation of fluorescently labeled $PI(4,5)P_2$, $PI(5)P$, and $PI(4)P$ by WT PRL-3. Phosphatase assays containing 1.0 μg of fluorescent phosphoinositide substrate were conducted for 1 h at 37 °C with 9 μg of recombinant PRL-3 or in the presence of buffer only. Shown is a representative result of three experiments.

by PRL-3, whereas there is a clear gap between the product and $PI(5)P$. This result provides support for PRL-3 being a phosphatidylinositol 5-phosphatase.

Further, molecular modeling of PRL-3 with $diC8-PI(4,5)P_2$ can support the feasibility of PRL-3's 5-phosphatase activity. The aim of our model study was to find the highest-scoring docking solution containing either the 4- or the 5-phosphate pointing toward the catalytically active Cys. Because there is no structure available for PRL-3 bound to a ligand, we performed homology modeling and MD simulation for model refinement using the structure of PRL-1 bound to a sulfate ion (PDB entry 1XM2) as a template.[26] The 3D structural model of $diC8-PI(4,5)P_2$ in the deprotonated form for molecular docking was built on the basis of the structure of $PI(3)P$ bound to

MTMR2.[36] During the entire process, Cys 104 was considered to be deprotonated and hence functions as a nucleophile in the catalytic reaction. Asp 72 was considered protonated and therefore able to act as a general acid in catalysis. One hundred docking solutions were generated and ranked by GoldScore. To select the possible binding mode, the complex structures of MTMR2 with $PI(3)P$ (PDB entry 1ZSQ) and $PI(3,5)P_2$ (PDB entry 1ZVR)[36] were used for reference. A common feature of the binding mode in these two structures is that the hydrogen on the carbon atom that carries the phospho group pointing into the catalytic site is opposite to the "general acid" residue Asp 422. The highest-scoring docking solution satisfying this feature was selected as the initial predicted binding mode (Figure 8A,B). In this docking solution, the 5-phosphate of $diC8-PI(4,5)P_2$ is dephosphorylated. To further test this preference, a constrained docking study was performed in which either the 4- or 5-phosphate was constrained in the catalytic pocket. Three parallel dockings were performed for each situation, and 10 docking solutions were generated in each run. Solutions satisfying the feature described above with the highest score in each run were selected for comparison. The results show that the scores for docking solutions in which the 5-phosphate points into the catalytic site are generally higher. The highest-scoring one, which also scores higher than the initial predicted binding mode, was selected as the final predicted binding mode (Figure 8C,D). These theoretical studies further corroborate the hypothesis that PRL-3 could be a phosphatidylinositol 5-phosphatase.

Investigation of the Influence of the Mutations on PRL-3's Ability To Promote Cell Migration. Next, we determined the cellular phenotype of WT PRL-3 and its variants. PRL-3-overexpressing cells are reported to enhance
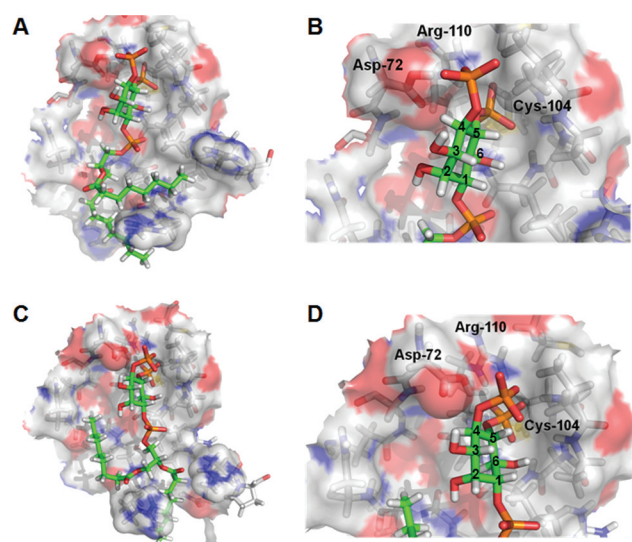
Figure 8. Docking solution of PI(4,5)P₂ bound to PRL-3. (A) Initial predicted binding mode. (B) Close-up of the catalytically active site of the structure in panel A. The 5-phosphate points toward Cys 104. (C) Final predicted binding mode, with the solution with the highest score. (D) Close-up of the catalytically active site of the structure in panel C.
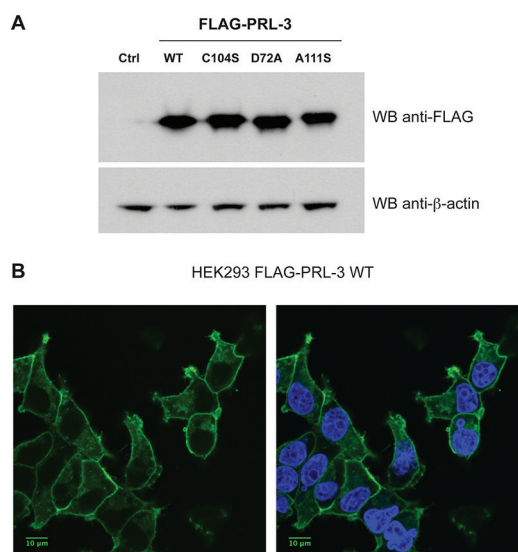

Figure 9. Generation of stable Flp-In T-Rex 293 cells expressing FLAG-tagged WT PRL-3 or its mutants under the control of a tetracycline inducible promoter. (A) Western blot (WB) analysis of cell lysates from stable cell lines expressing WT or mutant PRL-3. Cells were incubated overnight in medium containing 1 μg/mL tetracycline, harvested, lysed, and probed with an anti-FLAG antibody to assess the expression levels; an anti-β-actin antibody was used as a loading control. A control cell line was also generated by transfecting Flp-In 293 cells with the blank vector (Ctrl). (B) The stable cell lines were processed for indirect immunofluorescence using the FLAG antibody (left). Hoechst was used to stain the nuclei (right). Only WT PRL-3 is shown.
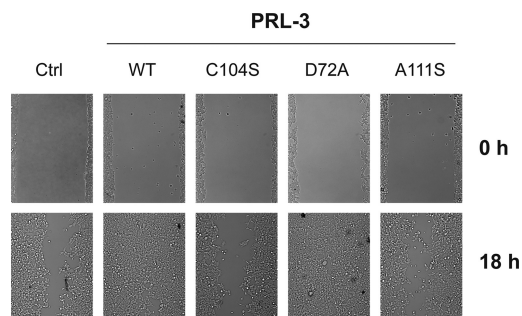
cell migration in a wound healing assay.[3,17] Thus, we created stable cell lines of all PRL-3 variants as well as WT PRL-3 and a stable control cell line with the empty vector using the Flp-In 293 T-Rex cell line (Invitrogen). All PRL-3 proteins were triple FLAG-tagged at the N-terminus. Anti-FLAG Western blot analysis showed that all PRL-3 cell lines express the proteins in equal amounts (Figure 9A), and immunofluorescence read-out with anti-FLAG antibodies shows that in all cell lines the proteins are localized equally to the plasma membrane as expected (shown for WT PRL-3 in Figure 9B, data of the variants not shown). There was no expression of PRL-3 observed in the control cell line.

We then conducted wound healing assays with all cell lines (Figure 10). As expected, the WT PRL-3 cell line closes the wound faster than the empty vector control cell line, demonstrating that WT PRL-3 promotes cell migration. The phenotype of the C104S PRL-3 cell line is the same as that of the empty vector control cell line, which is in agreement with the fact that the C104S mutant is inactive in vitro, and it also agrees with reports in the literature.[3,46] This indicates that PRL-3 catalytic activity is required to promote cell migration. The D72A PRL-3 cell line exhibited the same phenotype as WT PRL-3 cells. This correlates with the residual lipid phosphatase activity detected for this variant (see above). As discussed above, the D to A mutation does not completely inactivate the phosphatase, and given that D72A PRL-3 is highly overexpressed in our system, the residual catalytic activity of this variant could be sufficient for promoting cell migration. Fiordalisi et al. reported the same observation using stably transfected SW480 cells.[17] In another report, D72A PRL-3 transiently transfected into mouse B16 cells showed that the extent of promotion of cell migration in a Transwell assay was greatly reduced. However, some residual activity was observed compared to that of the C104S mutant and mock vector control.[46]

We made an astonishing observation when monitoring the cellular phenotype of the A111S mutant: It showed the same

Figure 10. Wound healing assay with stable HEK 293 cell lines expressing WT, C104S, D72A, and A111S PRL-3 as well as the empty vector control. Stable cell lines were incubated overnight in medium containing 1 μg/mL tetracycline to induce PRL-3 protein expression. A cell-free gap of approximately 500 μm was created by removing the Culture-Insert. The dishes were filled with fresh DMEM supplemented with 5% FBS and 1 μg/mL tetracycline to maintain protein expression. The wounded areas were photographed at the beginning of the assay (0 h, top panels) and after 18 h (18 h, bottom panels). Shown is a representative result of three experiments.

lack of activity in accelerating cell migration as the empty vector and the C104S mutant cell line. To the best of our knowledge, this mutant has never been tested in a wound healing assay. The hyperactivity toward the unnatural substrate, OMFP, is thus not apparent in the context of a living cell. On the other hand, the inactivity of A111S PRL-3 toward PI(4,5)P₂ in our in vitro assays is in complete agreement with the observed phenotype. This finding provides evidence that the natural S111A mutation in PRL-3 is required for its function, and it

might suggest that there are unknown mechanisms involved in the catalytic activity of the PRL family. It may also be that the A111S mutant no longer recognizes its natural substrate, which could potentially be due to structural perturbation in the variant. Importantly, our data clearly emphasize the need for caution when relating phosphatase activity with unnatural substrates such as OMFP to potential in cell activity.

To ensure that the activity of the recombinant protein really correlates with the enzyme when it is stably expressed in cells, all four PRL-3 proteins were immunoprecipitated and their phosphatase activity was analyzed using the fluorescently labeled PI(4,5)P$_2$. Figure 11 demonstrates that immunopreci-
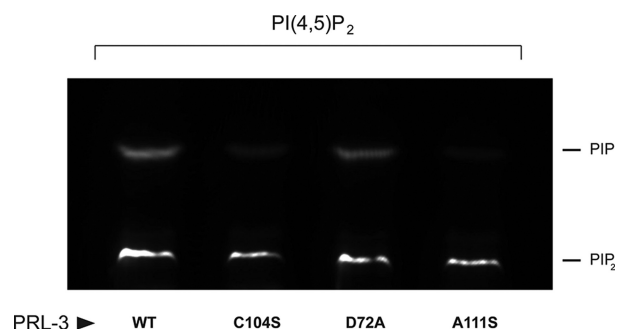

Figure 11. Dephosphorylation of fluorescently labeled PI(4,5)P$_2$ using immunoprecipitated WT, D72A, C104S, and A111S PRL-3. FLAG-tagged PRL-3 proteins were purified by immunoprecipitation with anti-FLAG affinity resin from HEK293 stable cell lines. Immunoprecipitates were incubated with 1.0 μg of fluorescently labeled PI(4,5)P$_2$ for 1 h at 37 °C, processed as described in Materials and Methods, and analyzed by TLC. Shown is a representative result of three experiments. Similar PIP background levels as in C104S and A111S PRL-3 lanes are also apparent in TLC read-outs using noninduced WT PRL-3 cells for immunoprecipitation (data not shown).

pitated WT and D72A PRL-3 can dephosphorylate PI(4,5)P$_2$, whereas the C104S and A111S variants lack phosphatase activity toward this substrate. These results are in complete agreement with the observed activity of the recombinant variants and also correlate with the observed phenotypes in wound healing assays.

Taken together, the monitored cellular phenotypes of all PRL-3 variants in stable HEK293 cell lines are in complete agreement with their activity toward PI(4,5)P$_2$ measured using two completely different biochemical assays. This suggests that this activity can be correlated to PRL-3's function in vivo.

CONCLUDING REMARKS

PRL-3 overexpression affects the regulation of multiple proteins and pathways leading to several favorable conditions for cancer progression and invasiveness.[2] Intriguingly, PI(4,5)P$_2$ plays a role upstream of many of the described signaling networks in which overexpressed PRL-3 exerts its activity. PI(4,5)P$_2$ is an important modulator of cytoskeleton organization during diverse cellular functions such as focal adhesion formation and cell migration. These dynamic processes require rapid and highly localized changes in PI(4,5)P$_2$ content; therefore, PI(4,5)P$_2$ levels are spatially and temporally regulated by the action of PI(4)P 5-kinases, 5-phosphatases, and phospholipase C enzymes (PLC).[43,47,48] Sequestration or depletion of membrane PI(4,5)P$_2$ decreases the plasma membrane–cytoskeletal adhesion energy leading to changes in cell shape,

reduction of cell–substrate adhesion, and formation of blebs.[49] Moreover, reduction of PI(4,5)P$_2$ levels through either hydrolysis by PLCγ or impairment of the PI(4,5)P$_2$-producing kinase PIPKIγ has been described as playing a role in cancer.[43] Depletion of PIPKIγ leads to a morphological transformation from an epithelial to a mesenchymal phenotype.[50] Reduction of PI(4,5)P$_2$ levels by PLCγ activates Cofilin-mediated enhanced cell motility.[43,48] Thus hypothetically, the role of PRL-3 in cancer metastasis and progression could be mediated via an effect on PI(4,5)P$_2$ levels.

PRL-3 is suggested to reduce the number of focal adhesions and/or increase the rate of focal adhesion turnover in cells leading to enhanced cell migration.[2] Focal adhesions are sites where cellular contact with the extracellular matrix is mediated by Integrins, and focal adhesion complexes contain more than 150 components.[43] Levels of PI(4,5)P$_2$ at the cell membrane are crucial for regulating the dynamics of focal adhesion complexes.[43] A key component of focal adhesion complexes is focal adhesion kinase (FAK), which integrates external signals to promote cell motility via many different pathways involving the regulation of or interaction with proteins such as Cadherins, Src, p130Cas, Rho-family GTPases, and Ezrin,[51] many of which have been implicated as being affected by or interacting with PRL-3.[1,2,10,11,13,14,16−18,20] Therefore, our finding that PRL-3 is active toward PI(4,5)P$_2$ offers a reasonable link to described effects of PRL-3 overexpression.

Little is known regarding the physiological role of PRL-3. If PRL-3 is a phosphatidylinositol 5-phosphatase, it would have to be tightly regulated in healthy cells given the importance of its potential substrate PI(4,5)P$_2$. PRL-3 is expressed only in low levels in specific tissues (skeletal muscle and heart),[1,2] which could be a hint about it being tightly regulated. In addition, its tight regulation has been described in the context of a nuclear function.[52] PIPs exist in the nucleus and regulate a number of processes such as chromatin remodeling and DNA repair; however, only one 5-phosphatase (SHIP2) has been reported in the nucleus, and its function is unclear.[6] In general, 10 human 5-phosphatases have been discovered to date, but none of them belongs to the superfamily of PTPs.[6] They conduct a variety of different functions and are regulated and expressed distinctly; however, our knowledge of regulatory mechanisms is in general still limited.[6,43] Alterations in these phosphatases lead to a number of diseases.[6,43] Their roles in cancer are very diverse and controversial, and they can range from tumor suppressors to cancer-promoting proteins, which was generally investigated in relation to their ability to dephosphorylate PI(3,4,5)P$_3$ to PI(3,4)P$_2$.[43]

These considerations make our hypothesis that PRL-3 could be a phosphatidylinositol 5-phosphatase very reasonable. Currently, we are working on the proof that PRL-3 has in vivo lipid phosphatase activity. Our results offer a new view of PRL-3's function and role and open up new lines of investigation for this important oncogene.

AUTHOR INFORMATION

Corresponding Author

*Telephone: +49 6221 3878544. Fax: +49 6221 387518. E-mail: koehn@embl.de.

Author Contributions

V.M. and G.V. contributed equally to this work.

■ ABBREVIATIONS

CD, circular dichroism; Csk, C-terminal Src kinase; DSP, dual-specificity phosphatase; EMT, epithelial−mesenchymal transition; FAK1, Focal Adhesion Kinase 1; GSK3β, Glycogen synthase kinase 3 β; GTPase, guanosine triphosphate hydrolase; IR, Insulin Receptor; JAK2, Janus Kinase 2; MD, molecular dynamics; OMFP, O-methylfluorescein phosphate; PDB, Protein Data Bank; PIP, phosphatidylinositol phosphate; PI3K, phosphoinositide 3-kinase; PRL, phosphatase of regenerating liver; PTEN, phosphatase and tensin homologue on chromosome 10; PTP, protein tyrosine phosphatase; 5-ptase, type IV 5-phosphatase; SHIP2, Src homology 2 domain-containing inositol phosphatase; Src, sarcoma; TLC, thin layer chromatography; WB, Western blot; WT, wild type.

■ REFERENCES

(1) Besette, D. C., Qiu, D., and Pallen, C. J. (2008) PRL PTPs: Mediators and markers of cancer progression. *Cancer Metastasis Rev.* 27, 231−252.

(2) Al-Aidaroos, A. Q., and Zeng, Q. (2010) PRL-3 phosphatase and cancer metastasis. *J. Cell. Biochem.* 111, 1087−1098.

(3) Zeng, Q., Dong, J. M., Guo, K., Li, J., Tan, H. X., Koh, V., Pallen, C. J., Manser, E., and Hong, W. (2003) PRL-3 and PRL-1 promote cell migration, invasion, and metastasis. *Cancer Res.* 63, 2716−2722.

(4) Matter, W. F., Estridge, T., Zhang, C., Belagaje, R., Stancato, L., Dixon, J., Johnson, B., Bloem, L., Pickard, T., Donaghue, M., Acton, S., Jeyaseelan, R., Kadambi, V., and Vlahos, C. J. (2001) Role of PRL-3, a human muscle-specific tyrosine phosphatase, in angiotensin-II signalling. *Biochem. Biophys. Res. Commun.* 283, 1061−1068.

(5) Saha, S., Bardelli, A., Buckhaults, P., Velculescu, V. E., St. Rago, C., Croix, B., Romans, K. E., Choti, M. A., Lengauer, C., Kinzler, K. W., and Vogelstein, B. (2001) A phosphatase associated with metastasis of colorectal cancer. *Science* 294, 1343−1346.

(6) Ooms, L. M., Horan, K. A., Rahman, P., Seaton, G., Gurung, R., Kethesparan, D. S., and Mitchell, C. A. (2009) The role of the inositol polyphosphate 5-phosphatases in cellular function and human disease. *Biochem. J.* 419, 29−49.

(7) Kim, K.-A., Song, J. S., Jee, J. G., Sheen, M. R., Lee, C., Lee, T. G., Ro, S., Cho, J. M., Lee, W., Yamazaki, T., Jeon, Y. H., and Cheong, C. (2004) Structure of human PRL-3, the phosphatase associated with cancer metastasis. *FEBS Lett.* 565, 181−187.

(8) Zeng, Q., Hong, W., and Tan, Y. H. (1998) Mouse PRL-2 and PRL-3, two potentially prenylated protein tyrosine phosphatases homologous to PRL-1. *Biochem. Biophys. Res. Commun.* 244, 421−427.

(9) Iwasaki, H., Murata, Y., Kim, Y., Hossain, Md. I., Worby, C. A., Dixon, J. E., McCormack, T., Sasaki, T., and Okamura, Y. (2008) A voltage-sensing phosphatase, Ci-VSP, which shares sequence identity with PTEN, dephosphorylates phosphatidylinositol 4,5-bisphosphate. *Proc. Natl. Acad. Sci. U.S.A.* 105, 7970−7975.

(10) Forte, E., Orsatti, L., Talamo, F., Barbato, G., De Francesco, R., and Tomei, L. (2008) Ezrin is a specific and direct target of protein tyrosine phosphatase PRL-3. *Biochim. Biophys. Acta* 1783, 334−344.

(11) Orsatti, L., Forte, E., Tomei, L., Caterino, M., Pessi, A., and Talamo, F. (2009) 2-D Difference in gel electrophoresis combined with Pro-Q Diamond staining: A successful approach for the identification of kinase/phosphatase targets. *Electrophoresis* 30, 2469−2476.

(12) Mizuuchi, E., Semba, S., Kodama, Y., and Yokozaki, H. (2009) Down-modulation of keratin 8 phosphorylation levels by PRL-3 contributes to colorectal carcinoma progression. *Int. J. Cancer* 124, 1802−1810.

(13) Peng, L., Jin, G., Wang, L., Guo, J., Meng, L., and Shou, C. (2006) Identification of integrin α1 as an interacting protein of protein tyrosine phosphatase PRL-3. *Biochem. Biophys. Res. Commun.* 342, 179−183.

(14) Peng, L., Xing, X., Li, W., Qu, L., Meng, L., Lian, S., Jiang, B., Wu, J., and Shou, C. (2009) PRL-3 promotes the motility, invasion, and metastasis of LoVo colon cancer cells through PRL-3-integrin β1-ERK1/2 and -MMP2 signaling. *Mol. Cancer* 8, 110−123.

(15) Zheng, P., Liu, Y.-X., Chen, L., Liu, X.-H., Xiao, Z.-Q., Zhao, L., Li, G.-Q., Zhou, J., Ding, Y.-Q., and Li, J. M. (2010) Stathmin, a new target of PRL-3 identified by proteomic methods, plays a key role in progression and metastasis of colorectal cancer. *J. Proteome Res.* 9, 4897−4905.

(16) Wang, H., Quah, S. Y., Dong, J. M., Manser, E., Tang, J. P., and Zeng, Q. (2007) PRL-3 down-regulates PTEN expression and signals through PI3K to promote epithelial-mesenchymal transition. *Cancer Res.* 67, 2922−2926.

(17) Fiordalisi, J. J., Keller, P. J., and Cox, A. D. (2006) PRL tyrosine phosphatases regulate rho family GTPases to promote invasion and motility. *Cancer Res.* 66, 3153−3161.

(18) Liang, F., Liang, J., Wang, W.-Q., Sun, J.-P., Udho, E., and Zhang, Z.-Y. (2007) PRL-3 Promotes Cell Invasion and Proliferation by Down-regulation of Csk Leading to Src Activation. *J. Biol. Chem.* 282, 5413−5419.

(19) Liang, F., Luo, Y., Dong, Y., Walls, C. D., Liang, J., Jiang, H.-Y., Sanford, J. R., Wek, R. C., and Zhang, Z.-Y. (2008) Translational control of C-terminal Src kinase (Csk) expression by PRL3 phosphatase. *J. Biol. Chem.* 283, 10339−10346.

(20) Liu, Y., Zhou, J., Chen, J., Gao, W., Le, Y., Ding, Y., and Li, J. (2009) PRL-3 promotes epithelial mesenchymal transition by regulating cadherin directly. *Cancer Biol. Ther.* 8, 1352−1359.

(21) Kozlov, G., Cheng, J., Ziomek, E., Banville, D., Gehring, K., and Ekiel, I. (2004) Structural Insights into Molecular Function of the Metastasis-associated Phosphatase PRL-3. *J. Biol. Chem.* 279, 11882−11889.

(22) Greenfield, N. J. (2007) Using circular dichroism spectra to estimate protein secondary structure. *Nat. Protoc.* 1, 2876−2890.

(23) Sun, J.-P., Luo, Y., Yu, X., Wang, W.-Q., Zhou, B., Liang, F., and Zhang, Z.-Y. (2007) Phosphatase Activity, Trimerization, and the C-terminal Polybasic Region Are All Required for PRL1-mediated Cell Growth and Migration. *J. Biol. Chem.* 282, 29043−29051.

(24) Pascaru, M., Tanase, C., Vacaru, A. M., Boeti, P., Neagu, E., Popescu, I., and Szedlacsek, S. E. (2009) Analysis of molecular determinants of PRL-3. *J. Cell. Mol. Med.* 13, 3141−3150.

(25) Traynor-Kaplan, A. E., Thompson, B. L., Harris, A. L., Taujor, P., Omann, G. M., and Sklar, L. A. (1989) Transient increase in phosphatidylinositol 3,4-bisphosphate and phosphatidylinositol tri-sphosphate during activation of human neutrophils. *J. Biol. Chem.* 264, 15668−15673.

(26) Jeong, D. G., Kim, S. J., Kim, J. H., Son, J. H., Park, M. R., Lim, S. M., Yoon, T. S., and Ryu, S. E. (2005) Trimeric structure of PRL-1 phosphatase reveals an active enzyme conformation and regulation mechanisms. *J. Mol. Biol. 345*, 401–413.

(27) The UniProt Consortium (2011) Ongoing and future developments at the Universal Protein Resource. *Nucleic Acids Res. 39*, D214–D219.

(28) Larkin, M. A., Blackshields, G., Brown, N. P., Chenna, R., McGettigan, P. A., McWilliam, H., Valentin, F., Wallace, I. M., Wilm, A., Lopez, R., Thompson, J. D., Gibson, T. J., and Higgins, D. G. (2007) Clustal W and Clustal X version 2.0. *Bioinformatics 23*, 2947–2948.

(29) Sun, J. P., Wang, W. Q., Yang, H., Liu, S., Liang, F., Fedorov, A. A., Almo, S. C., and Zhang, Z. Y. (2005) Structure and biochemical properties of PRL-1, a phosphatase implicated in cell growth, differentiation, and tumor invasion. *Biochemistry 44*, 12009–12021.

(30) Sali, A., and Blundell, T. L. (1993) Comparative protein modelling by satisfaction of spatial restraints. *J. Mol. Biol. 234*, 779–815.

(31) Zhou, H., and Zhou, Y. (2002) Distance-scaled, finite ideal-gas reference state improves structure-derived potentials of mean force for structure selection and stability prediction. *Protein Sci. 11*, 2714–2726.

(32) McGuffin, L. J. (2008) The ModFOLD server for the quality assessment of protein structural models. *Bioinformatics 24*, 586–587.

(33) Phillips, J. C., Braun, R., Wang, W., Gumbart, J., Tajkhorshid, E., Villa, E., Chipot, C., Skeel, R. D., Kale, L., and Schulten, K. (2005) Scalable molecular dynamics with NAMD. *J. Comput. Chem. 26*, 1781–1802.

(34) Wang, J. M., and Kollman, P. A. (2001) Automatic parameterization of force field by systematic search and genetic algorithms. *J. Comput. Chem. 22*, 1219–1228.

(35) Jorgensen, W. L., Chandrasekhar, J., Madura, J. D., Impey, R. W., and Klein, M. L. (1983) Comparison of Simple Potential Functions for Simulating Liquid Water. *J. Chem. Phys. 79*, 926–935.

(36) Begley, M. J., Taylor, G. S., Brock, M. A., Ghosh, P., Woods, V. L., and Dixon, J. E. (2006) Molecular basis for substrate recognition by MTMR2, a myotubularin family phosphoinositide phosphatase. *Proc. Natl. Acad. Sci. U.S.A. 103*, 927–932.

(37) Guha, R., Howard, M. T., Hutchison, G. R., Murray-Rust, P., Rzepa, H., Steinbeck, C., Wegner, J., and Willighagen, E. L. (2006) The Blue Obelisk—interoperability in chemical informatics. *J. Chem. Inf. Model. 46*, 991–998.

(38) Verdonk, M. L., Cole, J. C., Hartshorn, M. J., Murray, C. W., and Taylor, R. D. (2003) Improved protein-ligand docking using GOLD. *Proteins 52*, 609–623.

(39) Stephens, B., Han, H., Gokhale, V., and Von Hoff, D. (2005) PRL phosphatases as potential molecular targets in cancer. *Mol. Cancer Ther. 4*, 1653–1661.

(40) Jia, Z., Barford, D., Flint, A. J., and Tonks, N. K. (1995) Structural basis for phosphotyrosine peptide recognition by protein tyrosine phosphatase 1B. *Science 268*, 1754–1758.

(41) Rudolph, J., Epstein, D. M., Parker, L., and Eckstein, J. (2001) Specificity of natural and artificial substrates for human Cdc25A. *Anal. Biochem. 28*, 43–51.

(42) Wiland, A. M., Denu, J. M., Mourey, R. J., and Dixon, J. E. (1996) Purification and kinetic characterization of the mitogen-activated protein kinase phosphatase rVH6. *J. Biol. Chem. 271*, 33486–33492.

(43) Bunney, T. D., and Katan, M. (2010) Phophoinositide signalling in cancer: Beyond PI3K and PTEN. *Nat. Rev. Cancer 10*, 342–352.

(44) Kisseleva, M. V., Wilson, M. P., and Majerus, P. W. (2000) The Isolation and Characterization of a cDNA Encoding Phospholipid-specific Inositol Polyphosphate 5-Phosphatase. *J. Biol. Chem. 275*, 20110–20116.

(45) Blanchetot, C., Chagnon, M., Dubé, N., Hallé, M., and Tremblay, M. L. (2005) Substrate-trapping techniques in the identification of cellular PTP targets. *Methods 35*, 44–53.

(46) Wu, X., Zeng, H., Zhang, X., Zhao, Y., Sha, H., Ge, X., Zhang, M., Gao, X., and Xu, Q. (2004) Phosphatase of regenerating liver-3 promotes motility and metastasis of mouse melanoma cells. *Am. J. Pathol. 164*, 2039–2054.

(47) McLaughlin, S., Wang, J., Gambhir, A., and Murray, D. (2002) PIP(2) and proteins: Interactions, organization, and information flow. *Annu. Rev. Biophys. Biomol. Struct. 31*, 151–175.

(48) Saarikangas, J., Zhao, H., and Lappalainen, P. (2010) Regulation of the actin cytoskeleton-plasma membrane interplay by phosphoinositides. *Physiol. Rev. 90*, 259–289.

(49) Raucher, D., Stauffer, T., Chen, W., Shen, K., Guo, S., York, J. D., Sheetz, M. P., and Meyer, T. (2000) Phosphatidylinositol 4,5-bisphosphate functions as a second messenger that regulates cytoskeleton-plasma membrane adhesion. *Cell 100*, 221–228.

(50) Ling, K., Bairstow, S. F., Carbonara, C., Turbin, D. A., Huntsman, D. G., and Anderson, R. A. (2007) Type Iγ phosphatidylinositol phosphate kinase modulates adherens junction and E-cadherin trafficking via a direct interaction with μ1B adaptin. *J. Cell Biol. 176*, 343–353.

(51) Mitra, S. K., Hanson, D. A., and Schlaepfer, D. D. (2005) Focal adhesion kinase: In command and control of cell motility. *Nat. Rev. Mol. Cell Biol. 6*, 56–68.

(52) Basak, S., Jacobs, S. B. R., Krieg, A. J., Pathak, N., Zeng, Q., Kaldis, P., Giaccia, A. J., and Attardi, L. D. (2008) The metastasis-associated gene Prl-3 is a p53 target involved in cell-cycle regulation. *Mol. Cell 30*, 303–314.

■ NOTE ADDED AFTER ASAP PUBLICATION

This paper was published on the Web on August 11, 2011 with incorrect references in the caption of Table 1. The corrected version was reposted on August 15, 2011.